Accepted Manuscript

Ultrasensitive “signal-on” electrochemical aptasensor for assay of acetamiprid residues based on copper-centered metal-organic frameworks

Xueying Qiao, Fangquan Xia, Dong Tian, Peipei Chen, Jianhui Liu, Jinsong Gu, Changli Zhou

PII: S0003-2670(18)31331-X

DOI: https://doi.org/10.1016/j.aca.2018.11.004

Reference: ACA 236381

To appear in: *Analytica Chimica Acta*

Received Date: 10 June 2018

Revised Date: 30 October 2018

Accepted Date: 2 November 2018

Please cite this article as: X. Qiao, F. Xia, D. Tian, P. Chen, J. Liu, J. Gu, C. Zhou, Ultrasensitive “signal-on” electrochemical aptasensor for assay of acetamiprid residues based on copper-centered metal-organic frameworks, *Analytica Chimica Acta*, https://doi.org/10.1016/j.aca.2018.11.004.

Ultrasensitive “signal-on” electrochemical aptasensor for assay of acetamiprid residues based on copper-centered metal-organic frameworks

Xueying Qiao[a], Fangquan Xia[a], Dong Tian[a], Peipei Chen[a], Jianhui Liu[a], Jinsong Gu[b,*], Changli Zhou[a,*]

[a] Key Laboratory of Interfacial Reaction & Sensing Analysis in Universities of Shandong, School of Chemistry and Chemical Engineering, University of Jinan, Jinan 250022, P. R. China

[b] School of Biological Science and Technology, University of Jinan, Jinan 250022, P. R. China

*** Corresponding author：Changli Zhou and Jinsong Gu**

E-mail address:

chm_zhoucl@ujn.edu.cn (Changli Zhou) and gujs222@163.com (Jinsong Gu)

Tel.: +86 531 82765372

Fax: +86 531 82765969

Abstract

In present work, a versatile “signal-on” electrochemical aptasensor with ultra-sensitivity and high selectivity for detecting acetamiprid residues has been successfully constructed. Electrochemistry behaviors of as-synthesized copper-centered metal-organic frameworks (CuMOF) on various electrodes were investigated in details. The results indicated that CuMOF exhibited well-behaved redox events. Thus, we used Au-CuMOF as signaling element to label probe DNA (pDNA). The gold nanoparticles-reduced graphene oxide (Au-rGO) has a high specific surface area and excellent conductivity, which was utilized to immobilize complementary strand (cDNA). In the presence of acetamiprid, Au-CuMOF-labeled pDNA would hybridize with the exposed cDNA, allowing CuMOF to approach the electrode and produce a sensitive signaling current. Such a “signal-on” method does not suffer from the drawbacks of “signal-off” methods. The linear range of this proposed electrochemical aptasensor was 0.1 pM ~10.0 nM and the detection limit was as low as 2.9 fM. This platform exhibited wonderful selectivity, stability, and repeatability, and was successfully applied to detect acetamiprid residues in tea samples exhibiting enormous practical application potential.

Key words: acetamiprid; aptasensor; copper-centered metal-organic frameworks; biosensor

1. Introduction

Acetamiprid (N-[(6-chloro-3-pyridyl)methyl]-N′-cyano-N-methylacetamidine), as one of the broad-spectrum insecticides based on a nervous system attacking mechanism, has been widely applied to guarantee agricultural yield by destroying the insects, such as Hemiptera, Thysanoptera and Lepidoptera [1, 2]. However, inappropriate use of acetamiprid could cause [3, 4] potential health threat to people exposed to environments contaminated by acetamiprid[5, 6]. Thus, an eager demand arises for proposing new analytical methods of acetamiprid in agricultural products and the environment to reduce potential risks to people's health. Various analytical methods were applied to detect acetamiprid residues in practical samples such as high-performance liquid chromatography [7], gas chromatography [8], liquid/gas chromatography–mass spectrometry [9] and enzyme-linked immunosorbent assays [10]. However, these usual methods are complicated and labor-intensive. Besides, diverse expensive equipments are usually indispensable for those assays. These disadvantages limit the practical applications of these approaches in on-site and regular environmental monitoring. Electrochemical method assisted by photoirradiation has been considered as a potential novel technology due to it colligated the advantages of optical approaches and electrochemical sensors [11, 12]. Nevertheless, the relatively low selectivity of these sensors has restricted their application.

Aptasensors have recently aroused enormous attention in the field of pesticide detection owing to their advantages, such as low-cost, high selectivity and reproducible ability [13, 14]. Aptamer is a single-stranded DNA that can bind target forcefully and selectively [15, 16]. In varieties of aptasensors, electrochemical aptasensors are remarkable on account of their inherent merits such as high sensitivity and selectivity, quick response, cost-effective and high stability [17-19]. Although aptasensors possess a mass of positive attributes, majority probes of aptasensors work in a

signal-off pattern in which a measured current decreases along with the concentration of target increases. This signal-off mode severely hinders the gain of these sensors. In contrast, signal-on sensors are able to obtain much ameliorative signaling because the background current detected without target is reduced [20].

Recent research progresses in nanotechnology attract broad attentions. Nanoparticles exhibit their potentiality on working as fundamental building blocks or signaling elements of aptasensors [14]. Metal-Organic Frameworks (MOFs), with metal ions connected with branchy organic linkers, have ultrahigh specific areas and various functional groups (–COOH, $–NH_2$) [21, 22]. The majority of the research about MOFs has traditionally focused on gas storage materials [23], catalysis [24], drug release [25], and sensing [26]. Nevertheless, the application of many MOFs in electrochemical investigation is still faced tremendous difficulties on account of their inherent drawbacks such as the poor electron transfer capability and unsteadiness in aqueous environment [27, 28]. Yaghi et al. [29] developed a polyporous $Cu_3(BTB)_2(H_2O)_3 \cdot (DMF)_9(H_2O)_2$ (MOF-14) by means of utilizing 4,4′,4″-benzene-1,3,5-triyl-tribenzoic acid (H_3BTB) ligand and copper metal center. This compound is stable in air, insoluble in water or common organic solvents. Zhang et al. [30] investigated the electrochemical and electrocatalytic properties of MOF-14. Although copper-centered metal-organic frameworks (CuMOF) have excellent electrochemical activity and can generate a sensitive electrochemical signal, there have been few reports about using CuMOF as a signaling element of the biosensor.

Herein, a novel “signal-on” electrochemical aptasensor was developed for detecting acetamiprid sensitively and selectively. In this platform, dsDNA was formed owing to the hybridization between the aptamer and complementary strand (cDNA) which was immobilized on the surface of gold nanoparticles-reduced graphene oxide modified glassy carbon electrode

(Au-rGO/GCE). When acetamiprid presents, aptamers would release from Au-rGO/GCE and the cDNA is exposed. Therefore, Au-CuMOF-labeled probe DNA (pDNA) would hybridize with the exposed cDNA, making CuMOF draw near to the electrode surface where it could achieve electronic exchange, which produces a sensitive signaling current. This constructed electrochemical aptasensor detects acetamiprid successfully with a lower limit of detection of 2.9 fM. And the method has been applied to detect acetamiprid concentration in tea samples. The obtained results are satisfying which manifested that this aptasensor is an effective method for the determination of acetamiprid residues.

2. Experimental

2.1. Chemicals and apparatus

The acetamiprid aptamer (Apta) sequence of 5′-TGT AAT TTG TCT GCA GCG GTT CTT GAT CGC TGA CAC CAT ATT ATG AAG A-3′ was adopted from the reported literature [31]. The complementary strand (cDNA) with the sequence of 5'-SH-$(CH_2)_6$-CGC ATC GTT CTT CAT AAT ATG GTG TCA GCG ATC AAG AAC CGC TGC AGA CAA ATT ACA -3', and probe DNA (pDNA) with the sequence of 5'- TGA CAC CAT ATT ATG AAG AAC GAT GCG -$(CH_2)_6$-SH-3' were obtained from Shanghai Sangon Biotech Co., Ltd. All the DNA solutions (100 μM) were prepared in Tris–EDTA buffer (10 mM Tris–HCl, 1 mM EDTA, pH 8.0) and diluted to the desired concentration with the same Tris–EDTA buffer. Trimesic acid (TMA) (98%) was purchased from Shanghai Macklin Biochemical Co., Ltd. Graphite powder (spectral purity) was purchased from Sinopharm Chemical Reagent Co., Ltd. Acetamiprid, carbendazol, methamidophos, parathion-methyl, cypermethrin, deltamethrin, aldicarb and ethylparathion were purchased from Shanghai pesticide research institute co., LTD. All the rest reagents were of analytical grade. Ultrapure water (specific resistance of 18.2 MΩ·cm) obtained from a Heal-Force water purification

system was used throughout experiments.

Infrared spectrograms were obtained from a VERTEX 70 Fourier transform infrared spectrometer. Powder X-ray diffraction (XRD) pattern was tested on a Philips PW1710 instrument (Cu Kα radiation, 1.5418 Å). Scanning electron microscope (SEM) images and Energy Dispersive Spectrometer (EDS) were obtained using a field emission SEM (Zeiss, Germany). Transmission electron microscope (TEM) images were obtained using an H-800 microscope (Hitachi, Japan). Tea samples were pretreated by APLE-3000 automated pressurized liquid extractor (Beijing jitian instrument co. LTD). Electrochemical impedance spectra (EIS) were measured in the frequency region of 10^{5}-10^{-1} Hz with a voltage excitation amplitude of 5 mV on an IM6ex electrochemical workstation (ZAHNER, Germany). Cyclic voltammetry (CV) and differential pulse voltammetry (DPV) were carried out on a CHI760E electrochemical workstation (Shanghai Chenhua apparatus Co. Ltd) using a modified glassy carbon electrode as the working electrode, Ag/AgCl electrode as the reference electrode, and a platinum wire as the auxiliary electrode, respectively.

2.2 Synthesis of Au-rGO and Au-CuMOF

Ice-cold $NaBH_4$ (0.6 mL 0.1 M) was injected into a 20 mL solution containing 0.25 mM trisodium citrate salt and 0.25 mM $HAuCl_4$ under continuous stirring to obtain a mixed solution. The obtained mixture was stirred uninterruptedly for 6 h, and then AuNPs were produced [32].

The synthesis of graphene oxide (GO) conforms to a modified Hummers' method [33]. And the reduced graphene oxide (rGO) was obtained by reducing this GO with ascorbic acid [34]. Succinctly, graphite powder (1.0 g) was added into a round-bottomed flask containing sulfuric acid (40 mL) in an ice-bath. Then potassium permanganate (3.5 g) was gradually added to the above flask with gentle stirring. And keep stirring for 2 h, then the mixture was diluted with slow addition of water (150 mL) under stirring. Then the mixture was treated with hydrogen peroxide dropwise.

Filtered and washed the mixture with 10% hydrochloric acid. The obtained solid was dried in a vacuum oven at 60 □ for 72 h and GO was obtained. 10 mg of GO powder was dispersed in 100 mL of water. Then 100 mg of ascorbic acid was added to the dispersion with vigorous stirring at room temperature. The reduction progress continued for 48 h. Then the dispersion was dried and rGO was obtained.1mL rGO (1mg/mL) was added into 10mL AuNPs with stirring for 2 h to obtain Au-rGO.

CuMOF was prepared according to published literatures [35, 36]. A Trimesic acid (TMA) solution was obtained by dissolving 0.9981 g TMA in 50 mL water，and then NaOH solution was added into the solution by drops to adjust its pH value to 7.0. Next, 0.6342 g $CuCl_2$ was dissolved in 50 mL water to get a metallic solution. The metallic solution was put into the prepared TMA solution dropwise under constant stirring at a rate of 1000 rpm. Little by little, a blue precipitate appeared marking the formation of CuMOF. The blue mixture was continually stirred for 12 h, followed by centrifugation at 6000 rpm to obtain a blue precipitate. The blue precipitate was washed with ethanol three times, and dried at 70 ℃ for 5 h, followed by further drying for another 24 h at 110 ℃. The dried CuMOF was hermetically stored for further use. 10 mL CuMOF solution (2 mg/mL) was mixed with 10 mL AuNPs and stirred continuously for 3 h to obtain Au-CuMOF.

2.3 Preparation of pDNA/Au-CuMOF

The pDNA solution (500 μL, 10^{-7} M) was added into the Au-CuMOF solution (500 μL, 1 $mg \cdot mL^{-1}$) and kept overnight. The mixed solution was incubated with NaCl (100 μL, 2 M) for 24 h, which was followed by centrifugation with a rotation speed of 13000 rpm for 15 min. The supernatant was removed using a one-time dropper to get rid of free pDNA. The precipitate was washed twice with Tris-HCl buffer solution, and then was dispersed in Tris-HCl (10 mL, 50 mM).

2.4 Fabrication of electrochemical aptasensor and measurement of electrochemical signals

Scheme 1

The electrochemical aptasensor interface was established on a purified glassy carbon electrode (GCE) (ϕ=4.0 mm) as shown in Scheme 1. First, 10 μL Au-rGO dispersion solution was cast onto the GCE surface and desiccated under indoor temperature to obtain Au-rGO/GCE. Next, 5 μL cDNA (1.0×10^{-8} M) was dropped on the surface of Au-rGO/GCE and incubated at 40 □ for 1 h. Following that, the resulting electrode (cDNA/Au-rGO/GCE) was incubated with 16-mercapto-1-hexanol (MCH) for 60 min to block nonspecific binding sites. After that, the prepared MCH/cDNA/Au-rGO/GCE was incubated in 2 ml Apta solution at 40 □ for 40 min to form dsDNA between Apta and cDNA, obtaining Apta/MCH/cDNA/Au-rGO/GCE. Afterward, acetamiprid standard solutions with various concentrations were added to the surface of Apta/MCH/cDNA/Au-rGO/GCE at 60 □ for 120 min to make sure there was a complete reaction between Apta and acetamiprid. Finally, 5 μL pDNA/Au-CuMOF was dropped on the surface of the above electrodes, incubated for 40 min. These finished electrodes were ready for differential pulse voltammetry (DPV) measurement. After each step, the modified electrodes were adequately rinsed with Tris-HCl buffer to avoid the effects of physical adsorption.

DPV measurement was operated from -0.6 to 0.4 V (pulse amplitude = 50 mV, pulse width = 50 ms and pulse period = 0.5 s) and recorded the oxidation peak currents of CuMOF in the 0.1 M PBS solution (pH 7.0). The detection signal of the electrochemical aptasensor was relative to the acetamiprid concentration.

3. Results and discussion

3.1 Characterization of Au-rGO and Au-CuMOF

TEM was utilized to characterize the surface morphology of rGO and Au-rGO. The results were shown in Fig. 1A. rGO was uniformly distributed with evident wrinkles and typical layered structure with sheet-like morphology. After AuNPs were deposited onto the rGO, tiny dark dots with an average size of 30-40 nm were observed (Fig. 1B). TEM images of the Au-rGO exhibited better dispersion with equally allocated AuNPs, which was beneficial to the formation of robust homogeneous film for constructing electrochemical biosensor.

Fig.1

FT-IR and XRD were used to demonstrate the functional groups and crystal structure of CuMOF, severally. The results were displayed in Fig. 2. As we can see from Fig. 2A, the significant functional groups employed in MOF synthesis here were C=O at a frequency at about 1700 cm^{-1}. There were two divided peaks between 1500 and 1700 cm^{-1} indicating the interaction of carboxylate groups with Cu (II). The peak at 1150 cm^{-1} was attributed to –COOH stretching vibration whereas 496 and 730 cm^{-1} could be attributed to the Cu-O stretching vibration. There was also a quite important peak at about 933 cm^{-1} assigned to the -OH deformation peak of TMA. The XRD pattern (Fig. 2B) exhibited reflections of as-prepared CuMOF. Diffraction peaks at 2θ values of 6.7°，11.6° respectively represented (111) and (311) planes of crystal structure and all peaks in Fig. 2B were characteristic peaks of CuMOF according to the published literature [36].

SEM was utilized to further observe the morphology of CuMOF and Au-CuMOF. As we can see from Fig. 3A, CuMOF showed typical rod structure with a width of about 400 nm [35]. It was clear from Fig. 3B and C that AuNPs were evenly distributed on the CuMOF with an average diameter of about 10-20 nm. The energy-dispersive X-ray (EDS) was used to determine the

elemental composition of the Au-CuMOF (Fig. 2D). Results indicated that the as-prepared Au-CuMOF was composed of C, O, Cu and Au elements, which should be contained in Au-CuMOF exactly. The above results indicated CuMOF and Au-CuMOF were successfully prepared.

Fig.2

Fig.3

3.2 Electrochemical behaviors of Au-CuMOF

Cyclic voltammetry (CV) is the effective tool to characterize the electrochemical performances of different electrodes. Fig. 4 revealed the CV curves of bare GCE and different modified electrodes in PBS solution (pH 7.0). No redox peaks could be observed at the bare GCE (curve a). However, there was a pair of distinct redox peaks at the CuMOF/GCE (curve b). The oxidation peak (E_{pa}= -0.09 V) belonged to oxidizing reaction of Cu (0) and the reduction peak (E_{pc}= -0.24 V) belonged to reduction reaction of Cu (II) [22]. The peak-to-peak potential separation (ΔE_p) between the anodic peak and the cathodic peak was 113 mV, which indicated that the redox process of CuMOF was a quasi-reversible process. When the scan rates increased from 0.02 to 0.4 V/s, the redox currents increased obviously. Moreover, the redox currents were proportional to the arithmetic square root of the scan rate, revealing that the electrochemical processes were diffusion controlled processes. These results were also consistent with the previous report [30]. In comparison, redox peak currents of CuMOF/rGO/GCE (curve c) and CuMOF/Au-rGO/GCE (curve d) were successively larger due to rGO and Au-rGO possessing a larger specific surface area and better conductivity [37-39]. The electroconductibility was further improved, profiting from the introduction of AuNPs into CuMOF,

leading to the most sensitive electrochemical response generated by Au-CuMOF/Au-rGO/GCE (curve e). The redox peak current of CuMOF/Au-rGO/GCE decreased slowly and became stable finally as the following successive cyclic sweeps (Fig.4, inset). The relative standard deviation (RSD) was 3.5%, revealing acceptable stability of electrochemical behaviors of Au-CuMOF. Consequently, CuMOF can be used as the signaling element for the fabrication of electrochemical aptasensor.

Fig.4

3.3 Characterization of stepwise fabrication of the aptasensor

Fig. 5

EIS and DPV were employed to monitor each fabrication step of the electrochemical aptasensor. Fig. 5A displayed the EIS curves of different electrodes in 0.1 M KCl with 5 mM $K_3Fe(CN)_6$ /$K_4Fe(CN)_6$ (1:1) solution. The impedance spectrum contained a semicircle portion and a linear portion. The semicircle portion in the high-frequency region amounted to the charge-transfer limited process. A line portion observed at low frequencies corresponded to the diffusion process. As can be seen in Fig. 5A, the bare GCE exhibited a very small semicircle domain with the charge transfer resistances (R_{ct}) of 83.9 Ω (Fig.5A, curve a), indicating that the charge-transfer process of $[Fe(CN)_6]^{3-/4-}$ was very fast. When Au-rGO film was modified on the GCE, the value of Rct decreased to 59.1 Ω (Fig. 5A, curve b) benefited from the favorable electron transfer ability of Au-rGO [37-39]. Furthermore, the electron transfer behavior of bare GCE and

Au-rGO/GCE in $K_3Fe(CN)_6/K_4Fe(CN)_6$ solution were studied using cyclic voltammetry (CV). As shown in the Fig. 5B , a pair of well-defined redox peaks could be observed at both bare GCE and Au-rGO/GCE. The peak potential differences (ΔEp) of redox peaks on GCE was 0.082V (ΔEp=0.288-0.206=0.082 V). However, ΔEp on Au-rGO/GCE was 0.061V(ΔEp=0.279-0.218=0.061V), very close to the ideal value of 0.059 V. ΔEp was related to electron transfer coefficient [40], and a low ΔEp value indicates a fast electron transfer for a single-electron electrochemical reaction [41] on Au-rGO/GCE. This results were consistent with the characterization results of EIS. The R_{ct} values of cDNA/Au-rGO/GCE (Fig. 5A, curve c), MCH/cDNA/Au-rGO/GCE (Fig. 5A, curve d) and Apta/MCH/cDNA/Au-rGO/GCE (Fig. 5A, curve e) increased orderly with the step by step modification, which was due to the fact that cDNA, MCH and Apta were insulated hindering the electron transfer. After the Apta/MCH/cDNA/Au-rGO/GCE was incubated with 5 μL 0.1 nM acetamiprid solutions, the R_{ct} decreased. This was because aptamers were drawn down by the pesticide molecule and the hindrance to electron transfer reduced (Fig. 5A, curve f). When the signal probe pDNA/Au-CuMOF was coupled on the electrode surface, the R_{ct} increased due to the bad conductivity of pDNA/Au-CuMOF, making the electron transfer harder (Fig. 5A, curve g). An equivalent circuit diagram (the inset plot of Fig. 5A) was chosen to calibrate the plot in order to describe the impedance information of the modified electrodes in more detail (Rs, Q, Rct, and Zw respectively represented the resistance of the electrolyte solution, the double layer capacitance, the charge-transfer resistance and the Warburg impedance.). Besides, DPV characterization results in 0.1 M PBS solution (pH 7.0) were shown in the Fig. 5C. As we can see, there were no electrochemical responses in the steps a-f. When acetamiprid was added, the Au-CuMOF-labeled pDNA would combine with cDNA, allowing CuMOF to approach the electrode. A sensitive oxidation peak signaling current was produced at -0.09 V (Fig. 5C, curve g).

These results suggested that the sensitive “signal-on” electrochemical aptasensor had been successfully prepared.

3.4 Optimization of experimental conditions

As we all know, time and temperature have a significant effect on the analytical capability of sensors by affecting the combining capacity and activity of the DNA. For even better sensitivity and selectivity, the incubation time and temperature of cDNA with Apta, Apta with acetamiprid, cDNA with pDNA/Au-CuMOF were optimized, respectively. Three above relationships between oxidation peak current and time or temperature have been showed in Fig. 6.

Fig. 6

As is shown in the Fig. 6A, all the three peak currents increased along with the increase in incubation time. The oxidation peak currents (I_{pa}) resulted from the reaction of cDNA with Apta (curve a), Apta with acetamiprid (curve b), cDNA with pDNA/Au-CuMOF (curve c) reaching maximum values at 40, 120, and 40 min, respectively. The peak currents tended to flatten when the time increased beyond those points, which attributed to the three reactions needed a certain time. When the reaction was completely finished, the current won’t increase. Influences of incubation temperature of the above-mentioned three reactions were displayed in the Fig. 6B. Peak currents enhanced with temperature increase at the beginning, then reach maximums at 40, 60, and 40 □, respectively. After that, the three curves slightly declined or tended to be stable as the temperature continued rising. As the results showed, 40, 120, 40 min and 40, 60, 40 □ were selected in the next incubation experiments of cDNA with Apta, Apta with acetamiprid, and cDNA with pDNA/Au-CuMOF, respectively.

3.5 Analytical performances of the electrochemical aptasensor

The constructed electrochemical aptasensor was utilized to measure various concentrations of acetamiprid residue under the optimal reaction conditions. As we can see from Fig. 7, as the concentrations of acetamiprid incubated onto the aptasensor increased, the oxidation peak current (I_{pa}) around -0.09 V increased. The oxidation peak current was proportional to the logarithm of acetamiprid concentration in the large range of 0.1 pM to 10.0 nM with a linear regression equation of I_{pa} = *-703.15-55.07logc* (μA, M, R^2 = 0.999). And the limit of detection (S/N = 3) was 2.9 fMwhich is much lower than those early published (Table 1). The comparison showed that the constructed electrochemical aptasensor had better analytical performance for acetamiprid.

Fig.7

Table 1

3.6. Selectivity, reproducibility and stability of the proposed aptasensor

The selectivity of this constructed aptasensor was studied by testing the response of other substances similar in structure or function, such as carbendazol, methamidophos, parathion-methyl, cypermethrin, deltamethrin, aldicarb, and ethylparathion. The results were displayed in Fig. 8. It was found that no obvious oxidation peak appeared when the aptasensor was incubated with 1.0 nM carbendazol, methamidophos, parathion-methyl, cypermethrin, deltamethrin, aldicarb, ethylparathion, respectively. However, there appears a sensitive oxidation peak when 0.1 nM acetamiprid coexisted with the above several pesticides, and the peak current intensity of the mixture closely coincided with that of acetamiprid tested alone. Hence, the developed aptasensor

had excellent selectivity for acetamiprid. The reproducibility was evaluated by measuring 1.0 nM acetamiprid samples with five electrodes fabricated independently under the identical reaction conditions. The relative standard deviation (RSD) is 1.71%, indicating that reproducibility of the proposed aptasensor was acceptable. In addition, after the aptasensor was kept in a refrigerator at 4 °C for two weeks, over about 97% of the original current response was still retained, illustrating that the aptasensor had acceptable stability.

Fig. 8

3.7. Real sample analysis

The practicality of this constructed aptasensor for acetamiprid analysis in real samples was assessed. A series of tea samples from the local supermarket were tested by the established strategy. Same samples were also monitored using LC-MS in parallel. Tea samples were pretreated by accelerated solvent extraction (ASE). Selected tea samples (4.00 g) were ground into powders (40~60 mesh) and then transferred to extract cells. Acetone-dichloromethane (1: 1, V: V) served as the extraction solvent. And ASE variables were pressure (10.33 Mpa), temperature (100 □)，heat-up time（5 min）, static time (10 min), one extraction cycle. Then the extract cells were flushed with extraction solvent and purged by N_2 for 100 s. The collection liquid diluted to 25 ml with cyclohexane, and was ready to be used. The recovery experiment was performed using standard addition method. And recovery results were exhibited in Table 2. From the results, it was noticed that the recovery range was between 96% and 104%. Results gotten by this developed aptasensor were in accord with that of LC-MS, which was regarded as a referents method to detect acetamiprid. These results indicated that the proposed aptasensor could detect acetamiprid residues sensitively

and accurately in environment and tea matrices and possessed satisfactory ultimate practicability.

Table 2

Conclusions

In summary, a novel “signal-on” electrochemical aptasensor with favorable sensitivity and selectivity for detecting acetamiprid has been successfully constructed. In this strategy, the AuNPs/rGO modified electrode promoted the transfer of electrons. Moreover, it also afforded a large enough surface area for immobilizing cDNA. The as-prepared Cu-MOF performed favorable redox behaviors. Au-CuMOF labeled pDNA would hybridize exposed cDNA, allowing CuMOF to approach the electrode and produce a sensitive signaling current. Such a “signal-on” method does not suffer from the drawbacks of “signal-off” method, and could achieve a high sensitivity and a low detection limit of 2.9 fM. The proposed aptasensor provides the advantages including selectivity, reproducibility, and stability. Additionally, the aptasensor has been applied to detect acetamiprid in tea samples with desirable results. This work broadens the application field of MOF materials. Besides, it has great promise for the quantitative determination of other analytes in food safety and environmental monitoring fields.

Acknowledgements

This work was funded by Shandong Provincial Natural Science Foundation, China (ZR2017MB063), National Natural Science Foundation of China (NSFC) (No. 31370090), and Project of Key R&D of Shandong Province in China (No. 2015GSF121006).

References

[1] M.B. Afzal, S.A. Shad, N. Abbas, M. Ayyaz, W.B. Walker, Cross-resistance, the stability of acetamiprid resistance and its effect on the biological parameters of cotton mealybug, Phenacoccus solenopsis (Homoptera: Pseudococcidae), in Pakistan, Pest Manag Sci, 71 (2015) 151.

[2] Y. Tian, Y. Wang, Z. Sheng, T. Li, X. Li, A colorimetric detection method of pesticide acetamiprid by fine-tuning aptamer length, Anal. Biochem., 513 (2016) 87.

[3] H. Shi, G. Zhao, M. Liu, L. Fan, T. Cao, Aptamer-based colorimetric sensing of acetamiprid in soil samples: Sensitivity, selectivity and mechanism, J. Hazard. Mater., 260 (2013) 754.

[4] W. Wijaya, S. Pang, T.P. Labuza, L. He, Rapid detection of acetamiprid in foods using surface-enhanced Raman spectroscopy (SERS), J. Food Sci., 79 (2014) T743-747.

[5] L. Fan, G. Zhao, H. Shi, M. Liu, Z. Li, A highly selective electrochemical impedance spectroscopy-based aptasensor for sensitive detection of acetamiprid, Biosens. Bioelectron., 43 (2013) 12.

[6] H. Li, Y. Qiao, J. Li, H. Fang, D. Fan, W. Wang, A sensitive and label-free photoelectrochemical aptasensor using Co-doped ZnO diluted magnetic semiconductor nanoparticles, Biosens. Bioelectron, 77 (2016) 378.

[7] M. Lopez-Garcia, R. Romero-Gonzalez, M. Lacasana, A. Garrido Frenich, Semiautomated determination of neonicotinoids and characteristic metabolite in urine samples using TurboFlowTM coupled to ultra-high performance liquid chromatography coupled to Orbitrap analyzer, J. Pharm. Biomed. Anal., 146 (2017) 378.

[8] B. Zhang, X. Pan, L. Venne, S. Dunnum, S.T. McMurry, G.P. Cobb, T.A. Anderson,

Development of a method for the determination of 9 currently used cotton pesticides by gas chromatography with electron capture detection. Talanta, 75 (2008) 1055.

[9] M. Mateu-Sanchez, M. Moreno, F.J. Arrebola, J.L.M. Vidal, Analysis of acetamiprid in vegetables using gas chromatography-tandem mass spectrometry, Anal. Sci., 19 (2003) 701.

[10] Wanatabe, S., Ito, S., & Kamata, Y. Development of competitive enzymelinked immunosorbent assays (ELISAs) based on monoclonal antibodies for chloronicotinoid insecticides imidacloprid and acetamiprid. Anal. Chim. Acta, 427(2001), 211.

[11] Sharma, M. V. P., Sadanandam, G., Ratnamala, A., Kumari, V. D., & Subrahmanyam, M. An efficient and novel porous nanosilica supported TiO_2 photocatalyst for pesticide degradation using solar light. J. Hazard. Mater., 171(2009), 626.

[12] D. Jin, Q. Xu, L. Yu, A. Mao, X. Hu, A novel sensor for the detection of acetamiprid in vegetables based on its photocatalytic degradation compound, Food Chem., 194 (2016) 959.

[13] S. Eissa, M. Zourob, Selection and characterization of DNA aptamers for electrochemical. biosensing of carbendazim, Anal. Chem., 89 (2017) 3138.

[14] A. Verdian, Apta-nanosensors for detection and quantitative determination of acetamiprid-A pesticide residue in food and environment, Talanta, 176 (2018) 456.

[15] J. Yang, B. Dou, R. Yuan, Y. Xiang, Aptamer/protein proximity binding-triggered molecular machine for amplified electrochemical sensing of thrombin, Anal. Chem., 89 (2017) 5138.

[16] J. He, Y. Liu, M. Fan, X. Liu, Isolation and Identification of the DNA Aptamer Target to Acetamiprid, J. Agric. Food Chem., 59 (2011) 1582.

[17] L. Fan, G. Zhao, H. Shi, M. Liu, Z. Li, A highly selective electrochemical impedance spectroscopy-based aptasensor for sensitive detection of acetamiprid, Biosens. Bioelectron., 43 (2013) 12.

[18] Madianos, G. Tsekenis, E. Skotadis, L. Patsiouras, D. Tsoukalas, A highly sensitive impedimetric aptasensor for the selective detection of acetamiprid and atrazine based on microwires formed by platinum nanoparticles, Biosens. Bioelectron., 101 (2018) 268.

[19] P. Weerathunge, R. Ramanathan, R. Shukla, T.K. Sharma, V. Bansal, Aptamer-controlled reversible inhibition of gold nanozyme activity for pesticide sensing, Anal. Chem., 86 (2014) 11937.

[20] Aaron A.Rowe, Kelly N.Chuh, Arica A.Lubin, Erin A. Miller, Brett Cook, Daniel Hollis, Kevin W. Plaxco, Electrochemical biosensors employing an internal electrode attachment site and achieving reversible, high gain detection of specific nucleic acid sequences, Anal. Chem., 83 (2011) 9462.

[21] M. Chen, N. Gan, Y. Zhou, T. Li, Q. Xu, Y. Cao, Y. Chen, An electrochemical aptasensor for multiplex antibiotics detection based on metal ions doped nanoscale MOFs as signal tracers and RecJf exonuclease-assisted targets recycling amplification, Talanta, 161 (2016) 867.

[22] H. Hosseini, H. Ahmar, A. Dehghani, A. Bagheri, A.R. Fakhari, M.M. Amini, Au-SH-SiO2 nanoparticles supported on metal-organic framework (Au-SH-SiO2@Cu-MOF) as a sensor for electrocatalytic oxidation and determination of hydrazine, Electrochimica Acta, 88 (2013) 301.

[23] K. Sumida, D.L. Rogow, J.A. Mason, T.M. McDonald, E.D. Bloch, Z.R. Herm, T.H. Bae, J.R. Long, Carbon dioxide capture in metal organic frameworks, Chem. Rev., 112 (2012) 724.

[24] L. Zhu, X.Q. Liu, H.L. Jiang, L.B. Sun, Metal−organic frameworks for heterogeneous basic catalysis, Chem. Rev., 117 (2017) 8129.

[25] X. Du, R. Fan, L. Qiang, K. Xing, H. Ye, X. Ran, Y. Song, P. Wang, Y. Yang, Controlled Zn^{2+}-triggered drug release by preferred coordination of open active sites within functionalization indium metal organic frameworks, ACS Appl. Mater. Interfaces, 9 (2017)

28939.

[26] A. Azhdari Tehrani, L. Esrafili, S. Abedi, A. Morsali, L. Carlucci, D.M. Proserpio, J. Wang, P.C. Junk, T. Liu, Urea metal−organic frameworks for nitro-substituted compounds sensing, Inorg. Chem., 56 (2017) 1446.

[27] A. Morozan, F. Jaouen, Metal organic frameworks for electrochemical applications, Energy Environ. Sci., 5 (2012) 9269.

[28] S.S. Kaye, A. Dailly, O.M. Yaghi, J.R. Long, Impact of preparation and handling on the hydrogen storage properties of Zn_4O (1, 4-benzenedicarboxylate)$_3$ (MOF-5), J. Am. Chem. Soc., 129 (2007) 14176.

[29] B. Chen, M. Eddaoudi, S.T. Hyde, M. O'Keeffe, O.M. Yaghi, Interwoven metal-organic framework on a periodic minimal surface with extra-large pores. Science, 291 (2001) 1021.

[30] B. Yuan, J. Zhang, R.Zhang, H. Shi, X. Guo, Y.Guo, X. Guo, S. Cai and D. Zhang, Electrochemical and electrocatalytic properties of a stable Cu-based metal-organic framework, Int. J. Electrochem. Sci., 10 (2015) 4899.

[31] Z. Yang, J. Qian, X. Yang, D. Jiang, X. Du, K. Wang, H. Mao, K. Wang, A facile label-free colorimetric aptasensor for acetamiprid based on the peroxidase-like activity of hemin-functionalized reduced graphene oxide, Biosens Bioelectron, 65 (2015) 39.

[32] K. Liu, Y. Bai, L. Zhang, Z. Yang, Q. Fan, H. Zheng, Y. Yin, C. Gao, Porous Au−Ag nanospheres with high-density and highly accessible hotspots for SERS analysis, Nano Lett., 16 (2016) 3675-3681.

[33] S. Sarker, K.-S. Lee, H.W. Seo, Y.-K. Jin, D.M. Kim, Reduced graphene oxide for Pt-free counter electrodes of dye-sensitized solar cells, Solar Energy, 158 (2017) 42.

[34] J. Zhang, H. Yang, G. Shen, P. Cheng, J. Zhang, S. Guo, Reduction of graphene oxide via

L-ascorbic acid, Chem. Commun., 46 (2010) 1112.

[35] Sahiner, N., Sel, K., Ozturk, O.F., Demirci, S., Terzi, G., Facile synthesis and characterization of trimesic acid-Cu based metal organic frameworks, Appl. Surf. Sci., 314 (2014) 663.

[36] K. Schlichte, T. Kratzke, S. Kaskel, Improved synthesis, thermal stability and catalytic properties of the metal-organic framework compound $Cu_3(BTC)_2$, Micropor.mesopor.mat., 73 (2004) 81.

[37] S.-J. Li, T.-W. Chen, N. Xia, Y.-L. Hou, J.-J. Du, L. Liu, Direct electrochemistry of glucose oxidase on sulfonated graphene/gold nanoparticle hybrid and its application to glucose biosensing, J.solid state electr., 17 (2013) 2487.

[38] Y. Shao, J. Wang, H. Wu, J. Liu, I.A. Aksay, Y. Lin, Graphene based electrochemical sensors and biosensors: a review, Electroanalysis, 22 (2010) 1027.

[39] F. Akbar, M. Kolahdouz, S. Larimian, B. Radfar, H.H. Radamson, Graphene synthesis, characterization and its applications in nanophotonics, nanoelectronics, and nanosensing, J. Mater. Sci.-Mater. EL., 26 (2015) 4347.

[40] R. S. Nicholso, Theory and application of cyclic voltammetry for measurement of electrode reaction kinetics. Anal. Chem., 1965, 37, 1351.

[41] N. G. Shang, P. Papakonstantinou, M. McMullan, M. Chu, A. Stamboulis, A. Potenza, S. S. Dhesi, H. Marchetto, Catalyst□free efficient growth, orientation and biosensing properties of multilayer graphene nanoflake films with sharp edge planes. Adv. Funct. Mater., 2008, 18, 3506.

[42] D. Jiang, X. Du, L. Zhou, H. Li, K. Wang, New insights toward efficient charge-separation mechanism for high-performance photoelectrochemical aptasensing: enhanced charge-carrier lifetime via coupling ultrathin MoS_2 nanoplates with Nitrogen-doped, Graphene quantum dots,

Anal. Chem., 89 (2017) 4525.

[43] B. Lin, Y. Yu, R. Li, Y. Cao, M. Guo, Turn-on sensor for quantification and imaging of acetamiprid residues based on quantum dots functionalized with aptamer, Sensor actuat. B-chem., 229 (2016) 100.

[44] Y. Qi, F.R. Xiu, M. Zheng, B. Li, A simple and rapid chemiluminescence aptasensor for acetamiprid in contaminated samples: Sensitivity, selectivity and mechanism, Biosens. Bioelectron, 83 (2016) 243.

[45] K. Abnous, N.M. Danesh, M. Ramezani, M. Alibolandi, P. Lavaee, S.M. Taghdisi, Aptamer based fluorometric acetamiprid assay using three kinds of nanoparticles for powerful signal amplification, Microchimica. Acta, 184 (2017) 81.

[46] A. Fei, Q. Liu, J. Huan, J. Qian, X. Dong, B. Qiu, H. Mao, K. Wang, Label-free impedimetric aptasensor for detection of femtomole level acetamiprid using gold nanoparticles decorated multiwalled carbon nanotube-reduced graphene oxide nanoribbon composites, Biosens. Bioelectron, 70 (2015) 122.

[47] S.M. Taghdisi, N.M. Danesh, M. Ramezani, K. Abnous, Electrochemical aptamer based assay for the neonicotinoid insecticide acetamiprid based on the use of an unmodified gold electrode, Microchimica. Acta, 184 (2017) 499.

[48] Q. Liu, J. Huan, X. Dong, J. Qian, N. Hao, T. You, H. Mao, K. Wang, Resonance energy transfer from CdTe quantum dots to gold nanorods using MWCNTs/rGO nanoribbons as efficient signal amplifier for fabricating visible-light-driven “on-off-on” photoelectrochemical acetamiprid aptasensor, Sensor actuat. B-chem., 235 (2016) 647.

Figure captions

Scheme 1 Illustration of the preparation process for the proposed aptasensor.

Fig.1 TEM images of the as-prepared rGO (A) and Au-rGO (B).

Fig.2 FTIR spectra (A) and XRD pattern (B) of as-prepared CuMOF.

Fig.3 SEM images of as-prepared CuMOF (A) and Au-CuMOF (B and C); EDS spectra of Au-CuMOF (D).

Fig.4 CVs of bare GCE (a), CuMOF/GCE (b), CuMOF/rGO/GCE (c), CuMOF/Au-rGO/GCE (d) and Au-CuMOF/Au-rGO/GCE (e) in 0.1M PBS (pH 7.0) at a scan rate of 50 mV s^{-1}. Inset: successive cyclic voltammograms of CuMOF/Au-rGO/GCE.

Fig.5 EIS (A) and DPV (C) of different preparation steps of aptasensor. Inset: the equivalent circuit diagram of EIS. The CVs (B) of bare GCE and Au-rGO/GCE in 0.1 M KCl with 5 mM $K_3Fe(CN)_6/K_4Fe(CN)_6$ (1:1) solution. bare GCE (a); Au-rGO/GCE (b); cDNA/Au-rGO/GCE (c); MCH/cDNA/Au-rGO/GCE (d); Apta/MCH/cDNA/Au-rGO/GCE (e); Apta/MCH/cDNA/Au-rGO/GCE incubated with 5μL of 0.1nM acetamiprid solution (f); the testing electrode (Au-CuMOF/pDNA/cDNA/Au-rGO/GCE) (g).

Fig.6 The effects of the reaction time (A) and incubation temperature (B) of cDNA with Apta (a), Apta with acetamiprid (b) and cDNA with pDNA/Au-CuMOF (c).

Fig.7 (A) The DPV curves of the aptasensor at different concentrations of acetamiprid: 0 (a), 0.1 pM (b), 1 pM (c), 10 pM (d), 0.1nM (e), 1 nM (f) and 10 nM (g). (B) The corresponding linear calibration curve.

Fig.8 The specificity of the proposed aptasensor toward acetamiprid against other pesticides.

Table 1 Comparison of analytical properties of various acetamiprid sensors.

Table 2 The results for determination of acetamiprid in tea samples.

Scheme 1

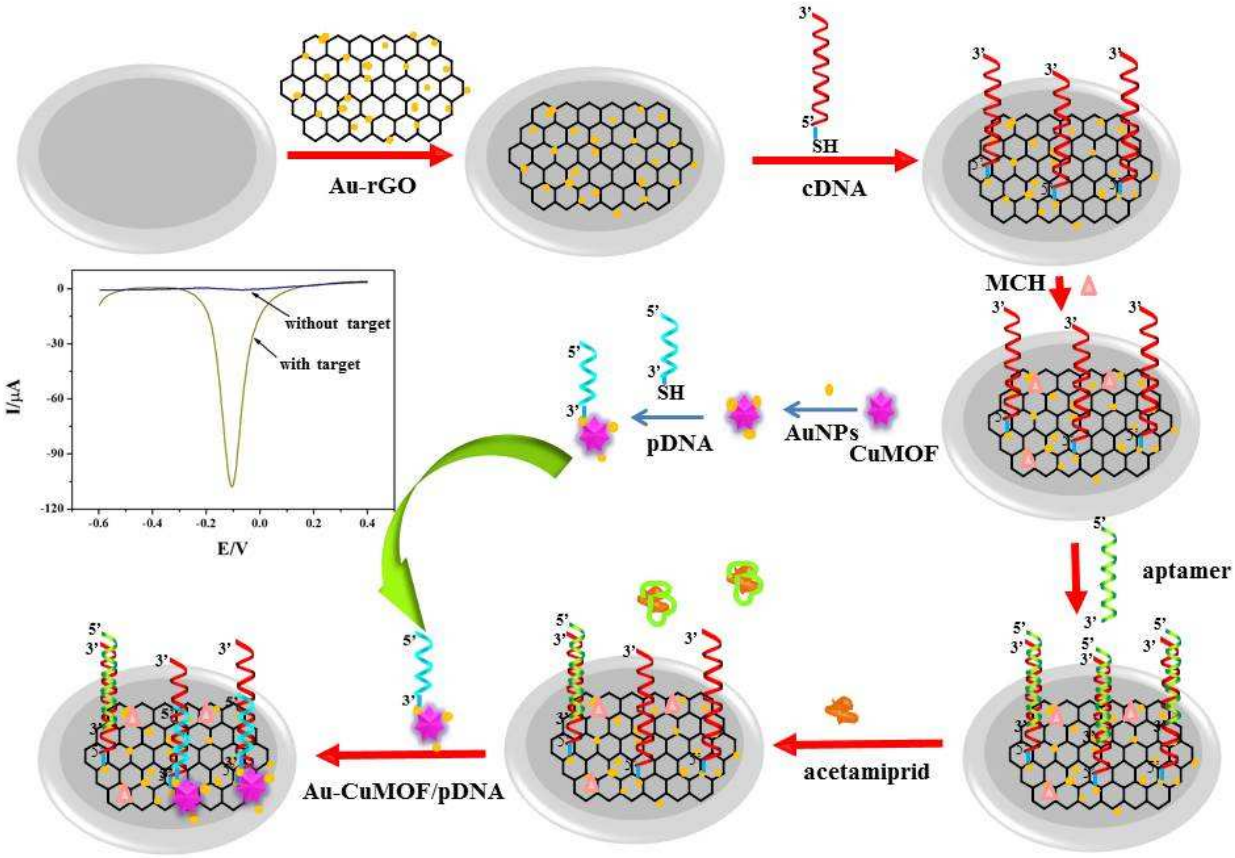

Fig. 1

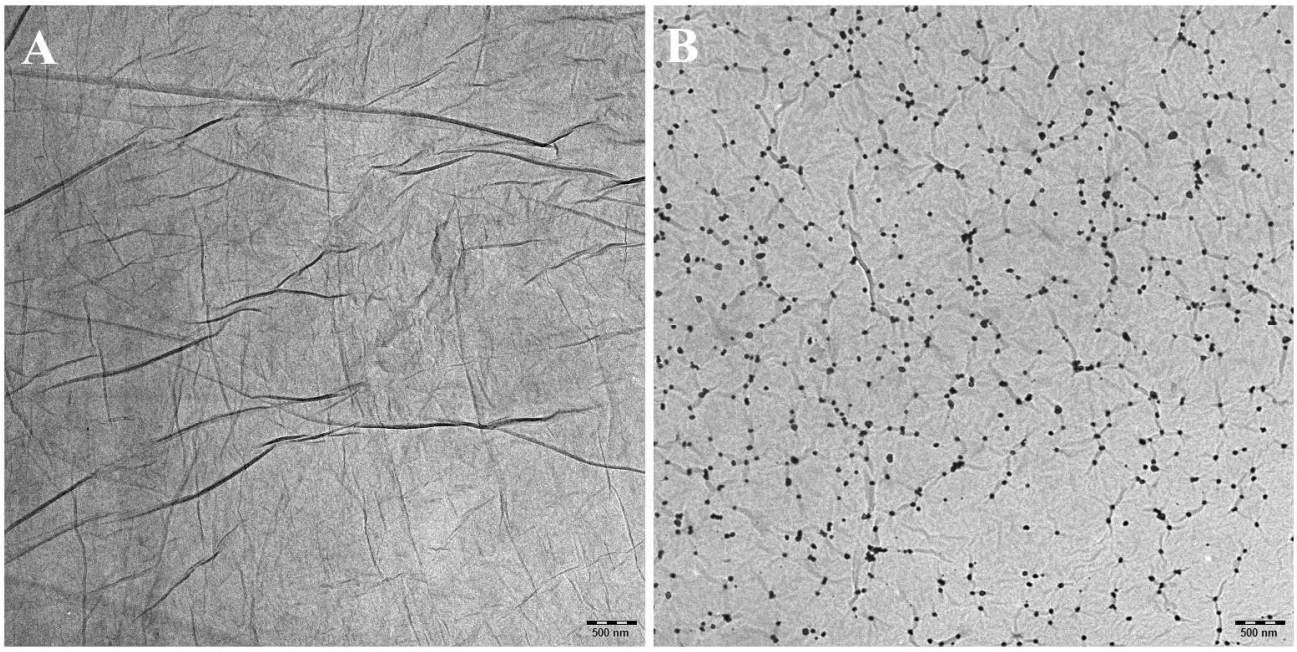

Fig. 2

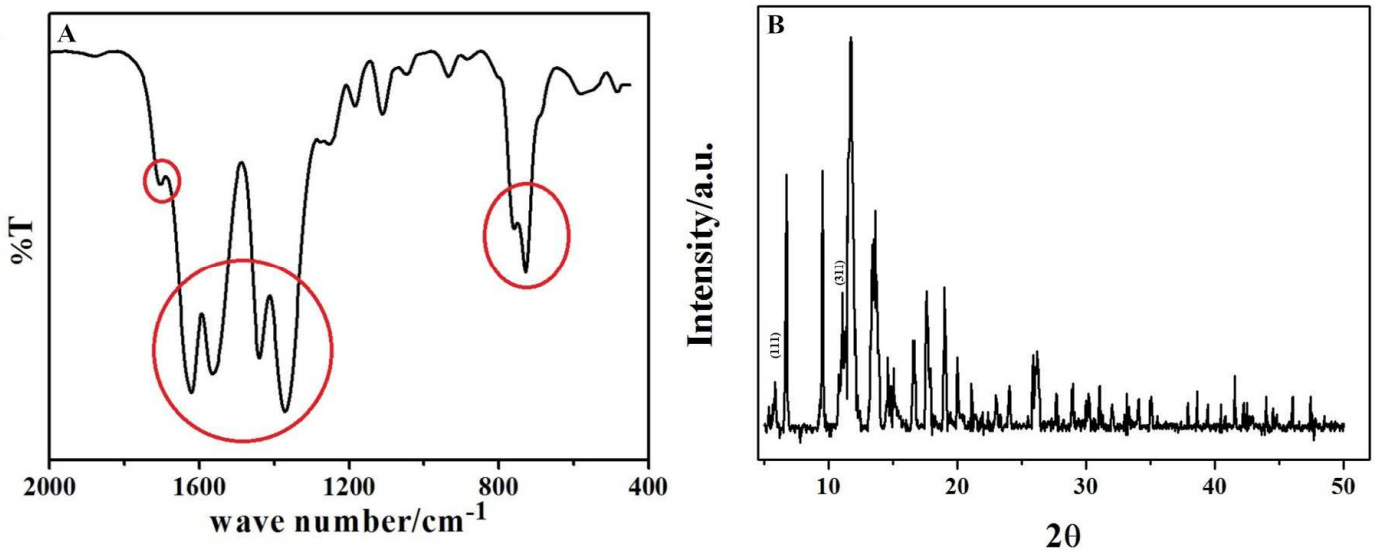
A
%T
2000
1600
1200
800
400
wave number/cm-1
B
Intensity/a.u.
(111)
(311)
10
20
30
40
50
2θ

Fig. 3

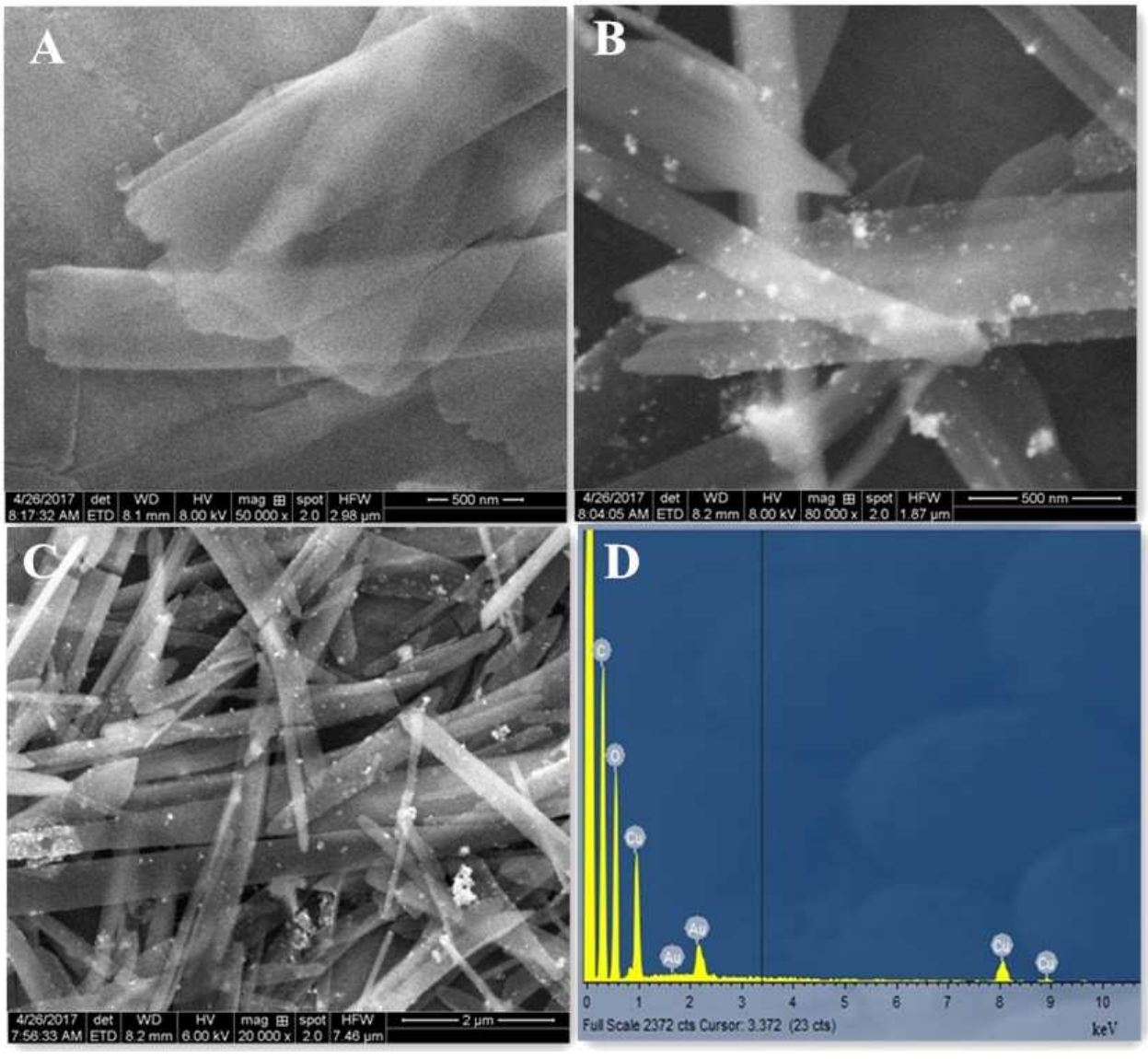
A
4/26/2017 8:17:32 AM det ETD WD 8.1 mm HV 8.00 kV mag 50 000 x spot 2.0 HFW 2.98 µm 500 nm
B
4/26/2017 8:04:05 AM det ETD WD 8.2 mm HV 8.00 kV mag 80 000 x spot 2.0 HFW 1.87 µm 500 nm
C
4/26/2017 7:58:33 AM det ETD WD 8.2 mm HV 6.00 kV mag 20 000 x spot 2.0 HFW 7.48 µm 2 µm
D
O
Cu
Au
Au
Cu
Cu
0 1 2 3 4 5 6 7 8 9 10
Full Scale 2372 cts Cursor: 3.372 (23 cts)
keV

Fig. 4

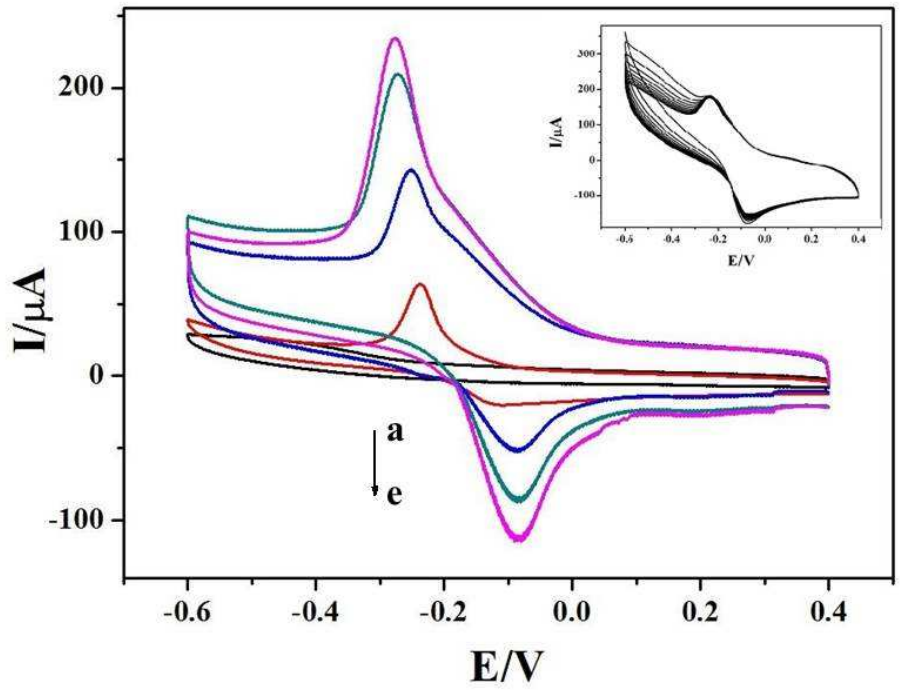
I/μA
E/V
a
e
I/μA
E/V

Fig. 5

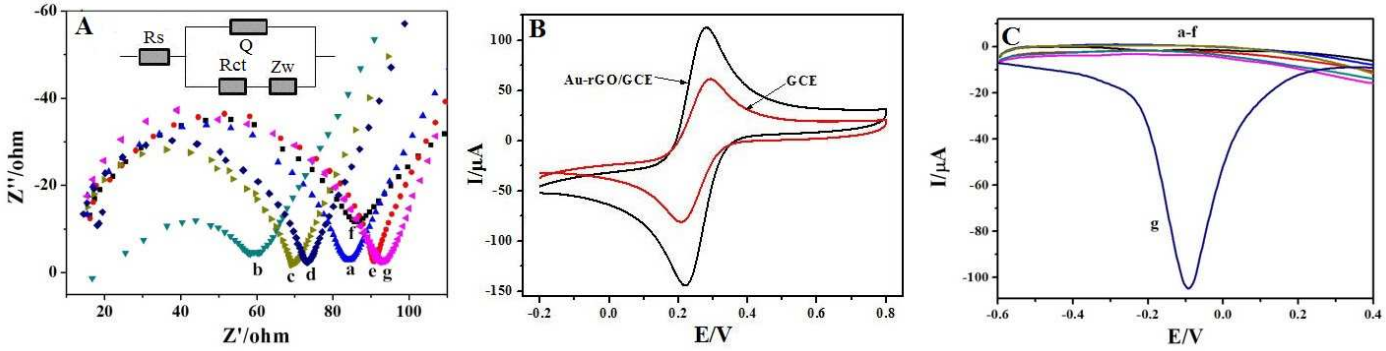
A
Rs
Q
Rct
Zw
Z''/ohm
Z'/ohm
B
Au-rGO/GCE
GCE
I/μA
E/V
C
a-f
g
I/μA
E/V

Fig. 6

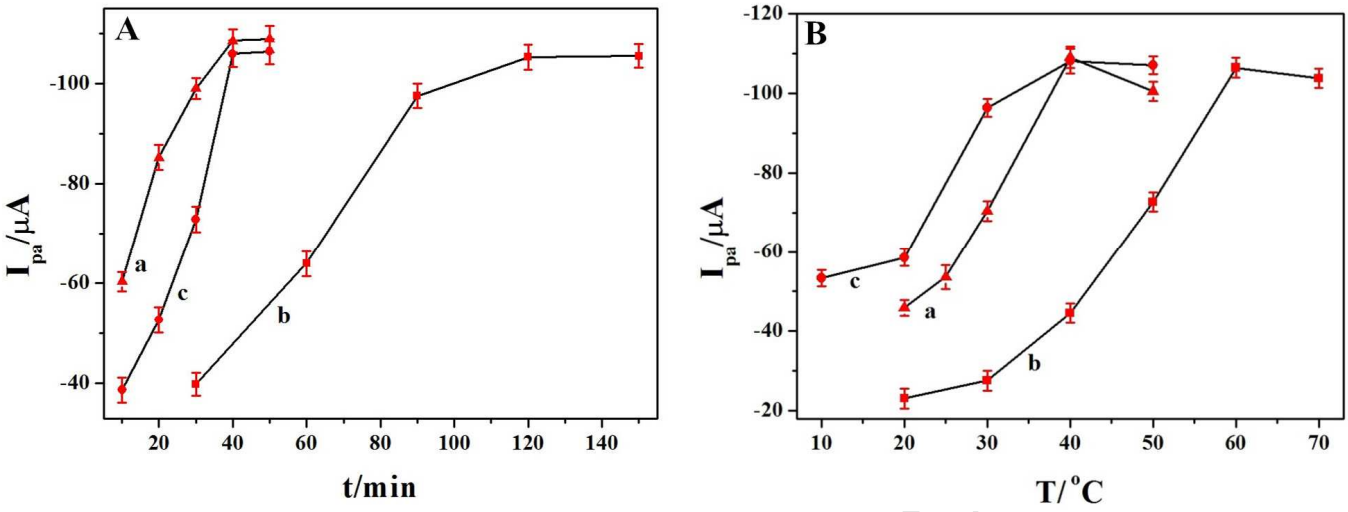

Fig. 7

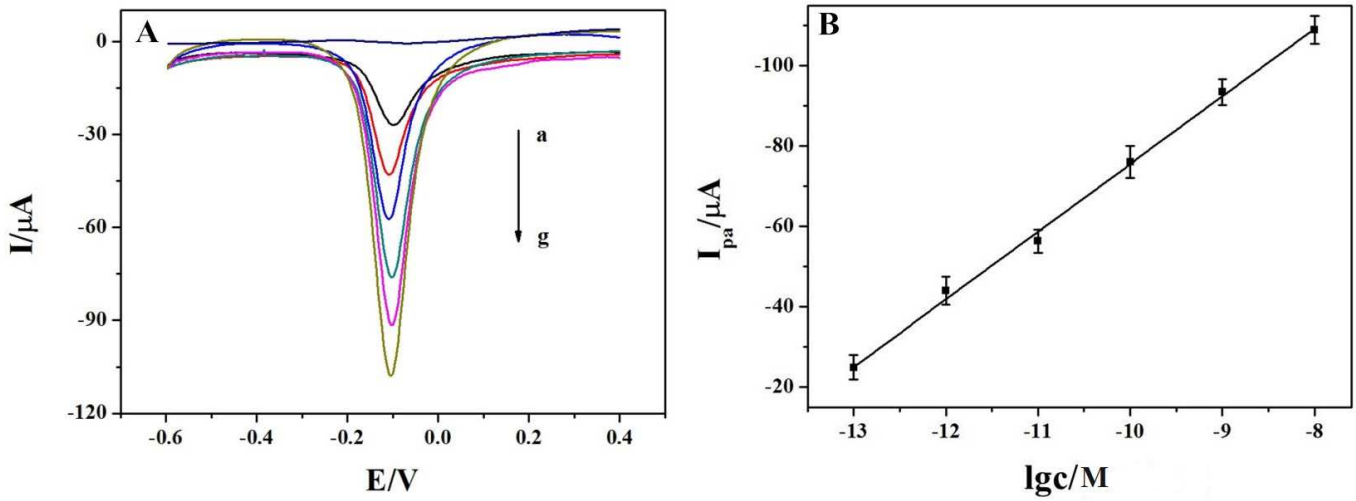

Fig. 8

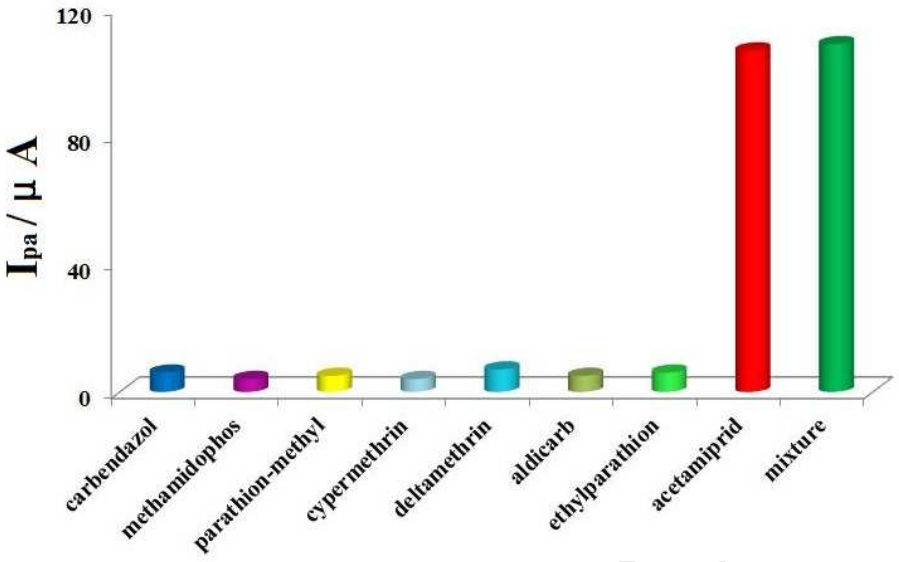

Table 1 Comparison of analytical properties of various acetamiprid sensors.

Detect method	strategy	LOD	Liner range	References
Colorimetry	GNPs-based colorimetric	0.4 μM	0~5.0 μM	[2]
Colorimetry	Aptamer-Controlled Reversible Inhibition of Gold Nanozyme Activity	0.1 ppm	0.1~10 ppm	[19]
PEC	Enhanced charge-Carrier lifetime	16.7 fM	0.05 pM to 1 nM	[42]
Fluorescence	FRET between ZnS: Mn-Aptamer and MWCNTs	0.7 nM	0 to 150 nM	[43]
Chemiluminescence	AuNPs morphology effects on CL	62 pM	0.8 to 630 nM	[44]
Fluorescence	three nanoparticles for signal amplification	127 pM	400 pM to 700 nM	[45]
EIS	Au/MWCNT-rGONR composites modified electrode	17 fM	50 fM to 10 μM	[46]
DPV	target-induced release of the redox probe	153 pM	0.5 to 650 nM	[47]
PEC	Resonance energy transfer from CdTe quantum dots to gold nanorods	0.2 pM	0.5pM to 10 μM	[48]
DPV	Au-CuMOF-labeled probe DNA,“signal-on” electrochemical aptasensors	2.9 fM	0.1 pM to 10.0 nM	This work

Table 2 The results for determination of acetamiprid in tea samples.

Sample		LC-MS (μg/g)	The aptasensor (n=3)				
			Determine value (μg/g)	Added (μg/g)	Total found (μg/g)	Recovery (%)	RSD (%)
Green tea	1#	-	-	0.05	0.051	102	3.2
	2#	-	0.001	0.05	0.049	96	4.1
	3#	0.03	0.029	0.05	0.080	102	4.6
Black tea	1#	-	-	0.05	0.048	96	2.5
	2#	0.07	0.068	0.05	0.120	104	5.7
	3#	0.04	0.042	0.05	0.091	98	3.9

Highlights:

1 A signal-on electrochemical acetamiprid aptasensor was fabricated.

2 CuMOF was prepared and used as a signaling element of aptasensor.

3 DNA reactions were ingeniously designed to improve the sensitivity.